5th International Conference on Experimental Fluid Mechanics ICEFM 2018 Munich
Munich, Germany, July 2-4, 2018

Laminar separation bubble on an SD7003 airfoil under large-scale turbulent inflow conditions

Sebastian L. Herbst[1*], Christian J. Kähler[1], Rainer Hain[1]

[1] Universität der Bundeswehr München, Institute of Fluid Mechanics and Aerodynamics, Neubiberg, Germany

[*] sebastian.herbst@unibw.de

Abstract

The flow field on the suction side of an SD7003 airfoil with a chord of $c = 0.2\,\mathrm{m}$ is investigated experimentally at a chord based Reynolds number of 60,000 for angles of attack between 4 and 16 degrees. Highly turbulent free-stream conditions were achieved by means of passive grids that produced a streamwise turbulent intensity of 10 %. Of special interest is the effect of the turbulent integral length scale, which is investigated for $L_{11} = c/2$ and $L_{11} = c$. The results show that the high turbulence intensity prevent the formation of laminar separation bubbles in the mean flow. However, instantaneous snapshots reveal separation bubbles at the leading edge, which occur with a higher probability as the angle of attack is increased. It is further shown that the high variation in size and shape of the separation bubble has a strong impact on the evaluated Reynolds stresses. Therefore a classification is introduced to perform statistics on the dataset.

1 Introduction

In recent years, there is a growing interest in low Reynolds number aerodynamics. Small aircrafts, often referred to as Micro Air Vehicles (MAV), are operated remotely or autonomously at Reynolds numbers between $Re = 50{,}000 \ldots 200{,}000$. This regime is significantly lower than the one classically studied since early pioneers like Ludwig Prandtl ($Re > 500{,}000$) and leads to a region of laminar flow on the airfoil surface. The majority of studies towards low Re aerodynamics focuses on the phenomenon of laminar separation, which occurs when the turbulence intensity Tu is low. During separation there is a reverse flow regime on the suction side of the airfoil which leads to significant changes in the lift to drag ratio, see Horton (1969); Gaster (1969); Ol et al. (2005); Radespiel et al. (2007); Hain et al. (2009); Kurelek et al. (2016); Yarusevych and Kotsonis (2017). At very low Re the laminar flow on the airfoil stays separated. However, when Re is increased, transition takes place in the separated shear layer, which leads to flow reattachment and the formation of a laminar separation bubble (LSB). This process was qualitatively shown to be very sensitive to initial conditions like acoustic noise or turbulence levels, see Ol et al. (2005); Kurelek and Yarusevych (2016).

Only a few systematic studies are available that address the influence of free-stream turbulence intensity. Lengani and Simoni (2015) and Lengani et al. (2017) studied a turbine blade airfoil up to $Tu = 5.2\,\%$ and applied POD in order to investigate the dynamics of the transition process. Simoni et al. (2017) investigated a thick flat plate airfoil up to $Tu = 2.87\,\%$ and Istvan and Yarusevych (2017) studied the influence of free-stream turbulence on a NACA0018 airfoil at four turbulence intensities ranging from $Tu = 0.11\,\%$ to $1.92\,\%$ with time resolved PIV and surface pressure measurements. Breuer (2018) investigated the flow over an SD7003 airfoil numerically for turbulent intensities up to $11.2\,\%$.

However, the turbulence intensity experienced during MAV flight can easily reach values larger than what has been previously investigated in the aforementioned citations. The flow regime close to the earth surface lies within the atmospheric boundary layer where the influence of friction and local ground conditions is present; especially in complex urban terrain turbulence intensities can reach values over 50 % (Ravi et al., 2012b). Taking the relative velocity of the flying aircraft into account, Tu values reduce, however still depending on wind conditions and terrain (Watkins et al., 2006). Replicating Tu reveals a very rough idea of the actual turbulent spectrum, which is characterized by the energy being distributed over a range of different scales. The latter can be estimated by the knowledge of the integral length scale L, which was shown to have

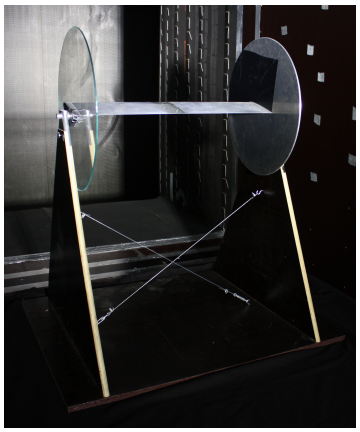

Figure 1: Wind tunnel model of an SD7003 airfoil with a chord of $c = 0.2\,\mathrm{m}$ and aspect ratio of 4.

a significant influence on a flat plate boundary layer (Fransson, 2017; Ravi et al., 2012a). Flying outdoors, MAVs experience a vast variety of sizes of turbulent structures from very small scales to large gusts with an expansion of several dozens of meters, which cannot be reproduced in wind tunnel experiments. The most influential turbulent strucutres are of the order $O(L_{11}) = c$, which can lead to varying forces along the airfoil axis and thus to rolling moments which are complicated to control. Statistically small distributed structures $O(L_{11}) << c$ tend to cancel out each other along the span and hence are not a significant problem. Larger structures lead to quasi static changes in the approaching flow and can be easily taken care of by an (auto-)pilot (Loxton, 2011; Fisher, 2013).

To the knowledge of the authors there is no literature available that address the effect of the integral length scale on a low *Re* airfoil, which is the main focus of the present study. The selected turbulent quantities for the free-stream are $Tu = 10\,\%$ and longitudinal integral length scales of $L_{11} = 0.1\,\mathrm{m}$ and $0.2\,\mathrm{m}$.

2 Experimental Setup

The Atmospheric Wind Tunnel Munich (AWM) is an open circuit Eiffel type wind tunnel with a test section of $1.85\,\mathrm{m} \times 1.85\,\mathrm{m}$ and a length of $22\,\mathrm{m}$. As outlined before, the free-stream flow properties are important for MAV aerodynamics and hence has to be carefully analyzed. Therefore, the streamwise velocity component was measured by a Dantec 55P15 probe, which was mounted on a traverse system. The hotwire signal was filtered at $4\,\mathrm{kHz}$ and then sampled at $8\,\mathrm{kHz}$ with an M2i.4652 Spectrum digitizer. In an open circuit wind tunnel, weather effects can disturb the signal on low frequencies and hence a high pass filter was used with a cut off frequency of $f_c = 0.1\,\mathrm{Hz}$. The baseline case, where no turbulence grids have been applied, showed a turbulence intensity of $Tu_{\mathrm{baseline}} = 0.5\,\%$.

In wind tunnels, appropriate turbulence can be produced by grids, placed at a certain distance in front of the measurement location. In principle, both active and passive grids can be used Roach (1987); Larssen and Devenport (2011). Passive grids are more restricted in the generated length scales but are easier to install in wind tunnels. They were already used by several authors in order to model atmospheric turbulence (Ravi et al., 2012a; Loxton, 2011) and hence have been selected for this project. The parameters Tu and L_{11} were changed by using different panel widths d and mesh lengths M (Roach, 1987). A general rule is that small turbulent length scales are produced by grids with small mesh lengths. However, along with M also Tu decreases. A solution to this limitation was found in using a second grid upstream, which lifts the overall turbulence to a higher level. With this a turbulent intensity of $Tu = 10\,\%$ was reached with integral length scales of $L_{11} = 0.1\,\mathrm{m}$ and $0.2\,\mathrm{m}$, respectively.

The investigated SD7003 airfoil was manufactured from aluminum with a chord length of $c = 0.2\,\mathrm{m}$ and an aspect ratio of 4. In order to minimize 3D effects, circular end plates with a diameter of $4\,c$ were mounted on each side, which is in agreement with Boutilier and Yarusevych (2012) who found that a diameter of $2.25\,c$ sufficiently suppresses 3D effects over a NACA0018 airfoil. One end plate was manufactured from glass in order to provide optical access to the airfoil for PIV measurements (s. Fig. 1).

The flow on the airfoil was measured by means of planar PIV (2D2C). In order to provide an overview, the suction side of the airfoil was completely captured by two PCO sCMOS cameras staggered along the

Table 1: PIV set-up parameters.

Parameter	baseline flow	turbulent flow	turbulent flow at leading edge
Light sheet thickness, mm	2	2	2
Sensor resolution, px	$2 \cdot (2560 \times 2160)$	$2 \cdot (2560 \times 2160)$	2560×2160
Field of view (combined), mm × mm	230×98	250×107	43×37
Δt, μs	120	90	30
Number of images	2000	3000	2000
Interrogation window, px	16	16	16
Overlap, %	50	50	75
Magnification, mm/px	0.047	0.050	0.017
Vector spacing, mm	0.379	0.399	0.068

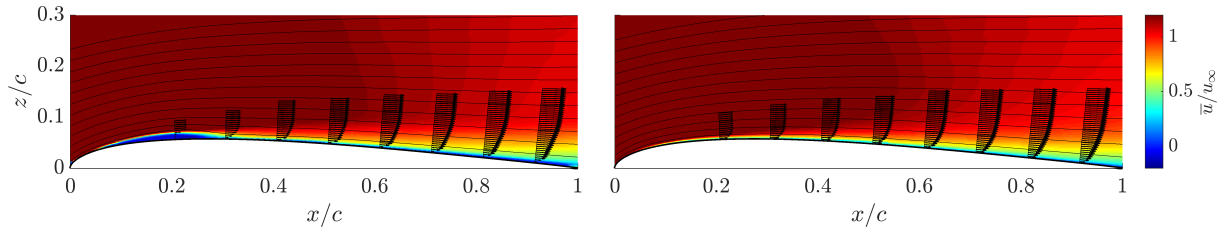

(a) Baseline flow with $Tu = 0.5\,\%$

(b) Turbulent free-stream conditions ($Tu = 10\,\%$, $L_{11} = 0.1\,\mathrm{m}$)

Figure 2: Mean flow field at an angle of attack of $\alpha = 8°$.

centerline at a Reynolds number of 60,000 and two angles of attack (4° and 8°). This setup was used for both the baseline flow and under elevated levels of turbulence. Detailed measurements under turbulent free-stream conditions were recorded by a single PCO sCMOS camera up to $\alpha = 16°$. This setup used a higher magnification and hence the field of view decreased to $x/c = 0 \ldots 0.18$ in streamwise direction. Details regarding the PIV parameters are provided in Table 1.

3 Results

The effect of elevated Tu on the flow field of the SD7003 airfoil is demonstrated by the contours in Fig. 2. The mean flow field for $L_{11} = 0.2\,\mathrm{m}$ and $\alpha = 8°$ is shown on the right. In comparison to the baseline case in Fig. 2(a) it is particularly noticeable that there is no LSB. The same holds for the flow with $L_{11} = 0.2\,\mathrm{m}$ as well as for both angles of attack which were investigated, though not explicitly shown here. Just recently Istvan and Yarusevych (2017) have investigated a NACA0018 airfoil at turbulence intensities between 0.1 % and 1.92 % and found that the mean bubble size decreases with increasing turbulence intensity, which is in agreement with the observations by Ol et al. (2005) and Olson et al. (2013). Breuer (2018) conducted LES with a synthetic turbulence inflow generator on the SD7003 airfoil and found that the LSB vanished for $Tu > 5.6\,\%$, when the mean flow field is considered. Hence the current recordings either prove that there is no laminar separation in the mean flow or the PIV recordings were not able to resolve the flow separation events in the boundary layer. This is also supported by pressure measurements as demonstrated by Herbst et al. (2018).

In order to achieve a higher resolution in the boundary layer the magnification of the PIV setup was roughly doubled as given in Table 1. With this setup angles of attack between 4° and 16° were observed. Representative snapshots of these measurements are given in Fig. 3. The figure reveals that there are instantaneous flow fields with separated shear layers. The observed flow structures in the boundary layer vary from a completely attached boundary layer in (a) to widely separated structures in (c). The snapshot shown in (b) looks very similar to a laminar separation bubble with transition to turbulence close to the rear part of the separated region.

As demonstrated in Fig. 5 there is a broad distribution of different sizes of separated areas, which are detected via a threshold on the streamwise velocity component. Three different thresholds for the binarization of the snapshots are compared, which do not show significant deviations, so that $u < 0.05\,u_\infty$ was selected

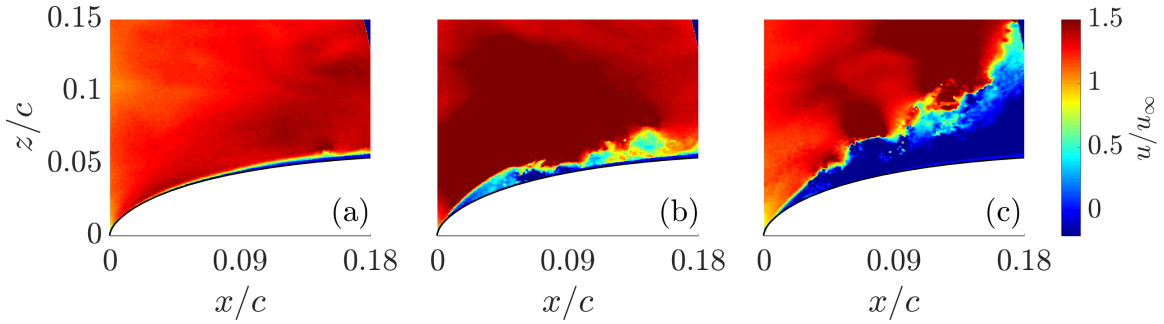

Figure 3: Independent snapshots of the boundary layer for showing different patterns in direct vicinity to the leading edge.

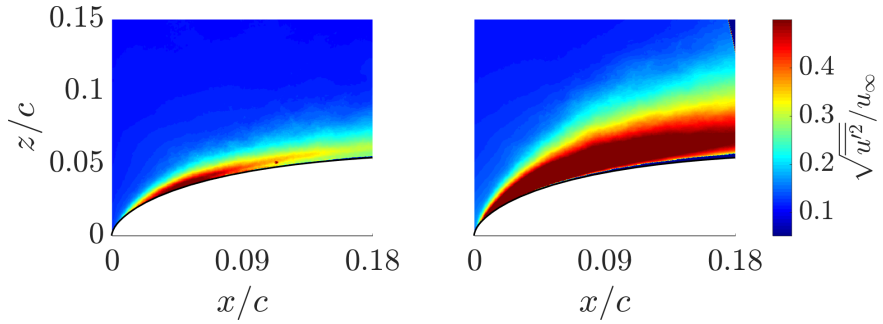

Figure 4: Streamwise Reynolds stresses $\overline{u'u'}$ for $\alpha = 8°$ (left) and $11°$ (right).

for the further analysis. The broad distribution leads to variations in the velocity field and high Reynolds stresses, respectively. However, the high $\overline{u'u'}$ values shown in Fig. 4 do not represent actual turbulence but rather are a consequence of the large-scale variations in the turbulent inflow.

Therefore additional data classification is needed before computing statistics. One feature for such a classification is the instantaneous angle of attack as discussed by Herbst et al. (2018). However, history effects are a big disadvantage of this kind of feature. Another possibility is to classify the velocity fields by means of the size of the separated region as already stated above. After visual inspection of Fig. 3 three classes are introduced in order to categorize the boundary layer, which are exemplarily represented by the subfigures (a) to (c). The PDF shows that most of the snapshots exhibit a very small area of slow streamwise velocity. Those are selected by a low-pass with a cutoff at $A/c^2 < 10^{-4}$. The second class, where a separation bubble is present, needs to be isolated by a threshold. Two different upper cutoff values are compared, which are $10^{-4} < A/c^2 < 6 \cdot 10^{-4}$ and $10^{-4} < A/c^2 < 18 \cdot 10^{-4}$. The class with relatively large separated areas is selected by a high-pass with a cutoff at $30 \cdot 10^{-4} < A/c^2$.

The percentage of snapshots within the proposed classes is given as a probability in Fig. 6, based on 2000 images per data set. It is shown that the angle of attack has a big impact on the boundary layer close to the leading edge. With rising α the probability of flow separation increases. At $\alpha = 4°$ almost all snapshots are sorted into the first class, which represents a fully attached boundary layer. Hence the probability of flow separation is close to zero. At $\alpha = 16°$ the probability of the first class drops to 5 %, which is equivalent with a probability of flow separation of around 95 %. Angles of attack of $\alpha = 8° \ldots 11°$ significantly promote the formation of small separated regions at a cost of fewer cases with a fully attached boundary layer. The probability for those separation bubbles shows a maximum and then drops since an increased α results in larger areas of separated flow, eventually leading to stall. As a broader threshold leads to more images in the particular case the plotted probability is slightly increased. Though, the overall characteristics are consistent. A larger integral length scale promotes the separation at all angles of attack. It is notable that at smaller angles of attack especially the formation of small separated areas is advanced.

The contours of the separated flow in Fig. 3 show similarities to laminar separation bubbles. Through visual inspection, the shear layer appears laminar before transition takes place with reattachment in the turbulent regime. Ol et al. (2005) use a threshold on the Reynolds shear stresses to define the location of

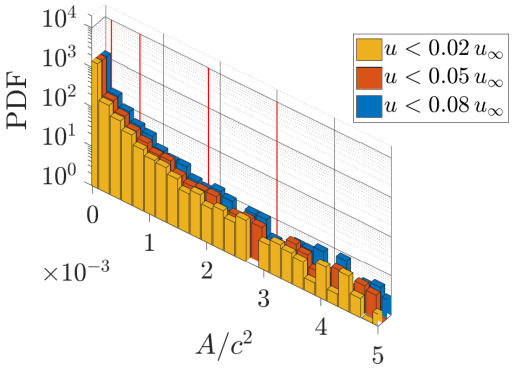

Figure 5: Probability density functions of the non-dimensional area of the separated region close to the leading edge at $L_{11} = 0.1\,\mathrm{m}$ and an angle of attack of $\alpha = 11°$.

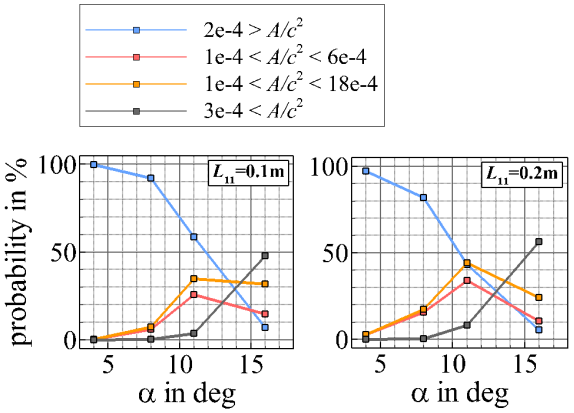

Figure 6: Probability of the occurrence of an area where $u < 0.05\,u_\infty$, which is used as a threshold for defining separated regions in the flow on the suction side close to the leading edge.

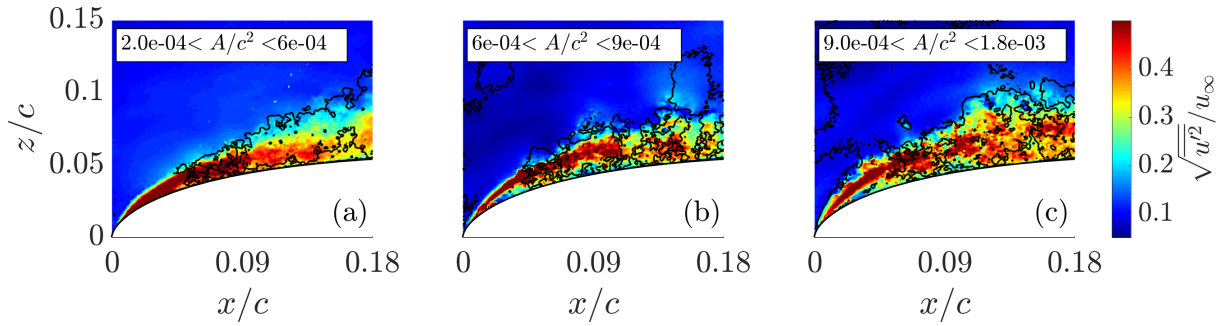

Figure 7: Streamwise Reynolds stresses $\overline{u'u'}$ after classification together with plotted contours of $\overline{u'v'} = -0.001$ at inflow conditions of $L_{11} = 0.1\,\mathrm{m}$ and $\alpha = 8°$.

transition x_{tr} where $-\overline{u'v'}$ reaches a value of 0.001 the first time. The corresponding contour is shown along with streamwise Reynolds stresses in Fig. 7 and indicates that the high $\overline{u'u'}$ at $x/c \leq 0.4$ are not caused by a turbulent boundary layer. Rather, they are the result of the high fluctuations in the oncoming flow, which interact with the evolving boundary layer and cause variations in the instantaneous angle of attack. This is supported by the snapshots in Fig. 8. Although the variations in the shape of the separated region were limited ($2 \cdot 10^{-4} < A/c^2 < 6 \cdot 10^{-4}$), there are significant differences, which are responsible for the high streamwise Reynolds stresses. For larger thresholds on A/c^2 the variations tend to move away from the airfoil while close to the surface a region of constant flow conditions develop below the separated shear layer. The averaged flow field of the streamwise velocity is given along with contours of the transition criterion in Fig. 9. The limited number of snapshots in the respective classes prevent a smooth contour, which makes quantitative analysis of the transition difficult. The overall characteristics, however, show good agreement with the baseline case, which is given in Fig. 9(d). Hence the classified flow fields prove that the separated regions in the various snapshots show instantaneous laminar separation bubbles.

4 Conclusion

The influence of large-scale free-stream turbulence on an SD7003 airfoil was examined for angles of attack between 4° and 16° at a Reynolds number of 60,000. Planar PIV (2D2C) was used to measure the flow field on the suction side of the airfoil.

Results show that there is no long separation bubble in the mean flow at angles of attack of 4° and 8°

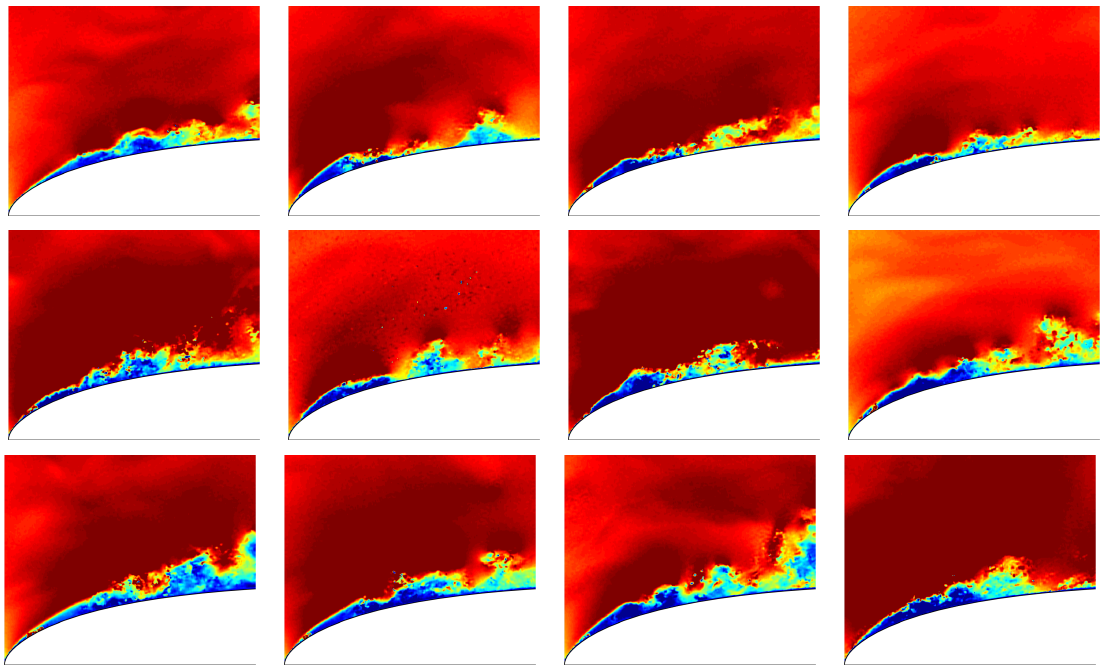

Figure 8: Instantaneous PIV Snapshots in turbulent free-stream conditions with $2 \cdot 10^{-4} < A/c^2 < 6 \cdot 10^{-4}$ at $L_{11} = 0.1\,\mathrm{m}$ and $\alpha = 8°$.

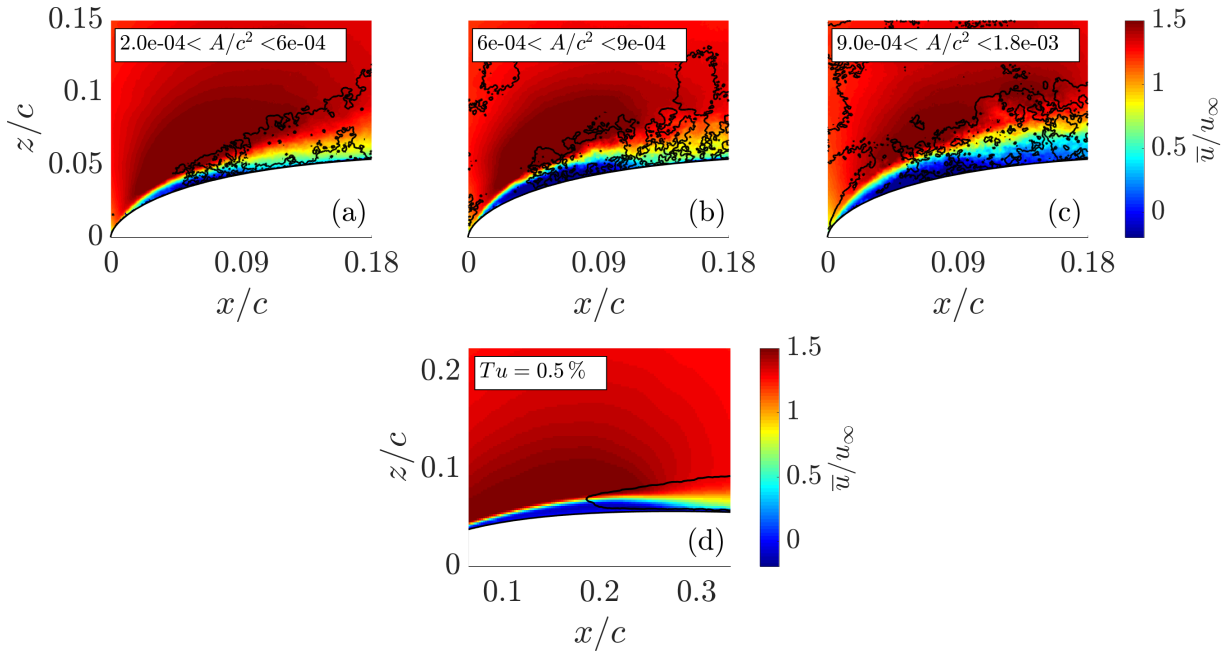

Figure 9: Reynolds stresses $\overline{u'u'}$ after classification together with plotted contours of $\overline{u'v'} = -0.001$ for $L_{11} = 0.1\,\mathrm{m}$ (a-c) and the baseline case (d) at $\alpha = 8°$.

when Tu is increased up to 10 percent. This is in agreement with recent numerical and experimental studies, which revealed that the LSB shrinks in size with increased turbulence intensities and eventually vanishes.

It is discussed that with large-scale turbulence there is a systematic effect of outer flow variations, which alters the boundary layer development. This can be attributed to large-scale disturbances. As a result, high turbulence levels appear in statistics when using standard methods for evaluating Reynolds stresses.

Measurements with a larger magnification close to the leading edge reveal the existence of instantaneous flow separation even at high levels of free-stream turbulence. A classification based on the size of the separated region showed that there is a certain probability of flow reattachment. Averaging on the classified data shows streamwise velocity contours, which are similar to laminar separation bubbles. Reynolds shear stresses showed good qualitative agreement with the baseline case in terms of the transition location. Therefore we can conclude that LSBs can still develop, when the level of free-stream turbulence intensity is raised. However, they do not occur permanently. Statistics show that the probability for this kind of boundary layer behavior depends on the angle of attack and the free-stream turbulence. An increased integral length scale raises the probability of short separation bubbles close to the leading edge. This might explain why LSBs are often not detected in time-averaged flow fields when Tu has been increased.

Acknowledgements

The authors gratefully acknowledge the German Research Foundation (DFG) for funding this work within the project HA 6926/2-1.

References

Boutilier MSH and Yarusevych S (2012) Parametric study of separation and transition characteristics over an airfoil at low reynolds numbers. *Experiments in Fluids* 52:1491–1506

Breuer M (2018) Effect of inflow turbulence on an airfoil flow with laminar separation bubble: An LES study. *Flow, Turbulence and Combustion*

Fisher AM (2013) *The effect of freestream turbulence on fixed and flapping micro air vehicle wings*. Ph.D. thesis. RMIT University. Melbourne, Australia

Fransson JHM (2017) Free-stream turbulence and its influence on boundary-layer transition. in *10th TSFP*. Chicago, USA

Gaster M (1969) *The structure and behaviour of laminar separation bubbles*. R&M 3595. ARC

Hain R, Kähler CJ, and Radespiel R (2009) Dynamics of laminar separation bubbles at low-reynolds-number aerofoils. *Journal of Fluid Mechanics* 630:129–153

Herbst SL, Kähler CJ, and Hain R (2018) Influence of large-scale free-stream turbulence on an SD7003 airfoil at low reynolds numbers. in *48th AIAA Fluid Dyn. Conf.*. Atlanta, USA

Horton H (1969) *A semi-empirical theory for the growth and bursting of laminar separation bubbles*. CP 1073. ARC

Istvan MS and Yarusevych S (2017) Free-stream turbulence effects on transition within a laminar separation bubble. in *47th AIAA Fluid Dyn. Conf.*. Denver, USA

Kurelek J and Yarusevych SV (2016) The effect of acoustic excitation on the later stages of transition in a laminar separation bubble. in *46th AIAA Fluid Dyn. Conf.*. number 3948 in AIAA AVIATION Forum. American Institute of Aeronautics and Astronautics, Washington, D.C., USA

Kurelek JW, Lambert AR, and Yarusevych S (2016) Coherent structures in the transition process of a laminar separation bubble. *AIAA Journal* 54:2295–2309

Larssen JV and Devenport WJ (2011) On the generation of large-scale homogeneous turbulence. *Experiments in Fluids* 50:1207–1223

Lengani D and Simoni D (2015) Recognition of coherent structures in the boundary layer of a low-pressure-turbine blade for different free-stream turbulence intensity levels. *International Journal of Heat and Fluid Flow* 54:1–13

Lengani D, Simoni D, Ubaldi M, Zunino P, and Bertini F (2017) Experimental study of free-stream turbulence induced transition in an adverse pressure gradient. *Experimental Thermal and Fluid Science* 84:18–27

Loxton B (2011) *An experimental investigation into the effects of atmospheric turbulence on the aerodynamics of micro air vehicle wings*. Ph.D. thesis. RMIT University. Melbourne, Australia

Ol MV, McAuliffe BR, Hanff ES, Scholz U, and Kähler CJ (2005) Comparison of laminar separation bubble measurements on a low reynolds number airfoil in three facilities. in *35th AIAA Fluid Dyn. Conf.*. 5149. Toronto, Canada

Olson DA, Katz AW, Naguib AM, Koochesfahani MM, Rizzetta DP, and Visbal MR (2013) On the challenges in experimental characterization of flow separation over airfoils at low reynolds number. *Experiments in Fluids* 54:1470

Radespiel R, Windte J, and Scholz U (2007) Numerical and experimental flow analysis of moving airfoils with laminar separation bubbles. *AIAA Journal* 45:1346–1356

Ravi S, Watkins S, Watmuff J, Massey K, Petersen P, Marino M, and Ravi A (2012a) The flow over a thin airfoil subjected to elevated levels of freestream turbulence at low reynolds numbers. *Experiments in Fluids* 53:637–653

Ravi S, Watkins S, Watmuff J, Massey K, Peterson P, and Marino M (2012b) Influence of large-scale freestream turbulence on the performance of a thin airfoil. *AIAA Journal* 50:2448–2459

Roach P (1987) The generation of nearly isotropic turbulence by means of grids. *International Journal of Heat and Fluid Flow* 8:82–92

Simoni D, Lengani D, Ubaldi M, Zunino P, and Dellacasagrande M (2017) Inspection of the dynamic properties of laminar separation bubbles: free-stream turbulence intensity effects for different reynolds numbers. *Experiments in Fluids* 58:66

Watkins S, Milbank J, Loxton B, and Melbourne W (2006) Atmospheric winds and their implications for microair vehicles. *AIAA Journal* 44:2591–2600

Yarusevych S and Kotsonis M (2017) Steady and transient response of a laminar separation bubble to controlled disturbances. *Journal of Fluid Mechanics* 813:955 – 990